JOURNAL OF CATALYSIS 69, 475–486 (1981)

# Surface Properties and Reduction Behavior of Calcined $CuO/Al_2O_3$ and $CuO–NiO/Al_2O_3$ Catalysts

REINHARD HIERL, HELMUT KNÖZINGER,[1] AND HANS-PETER URBACH

*Institut für Physikalische Chemie, Universität München, Sophienstrasse 11, 8000 München 2, West Germany*

Received October 6, 1980; revised January 19, 1981

The surface properties of copper and mixed copper–nickel aluminates have been investigated by means of optical spectroscopy, magnetic susceptibility, gravimetric carbon monoxide adsorption, thermal desorption, and infrared spectroscopy of adsorbed CO. $Cu^{2+}$ ions are exposed in the surface of the aluminates, while $Ni^{2+}$ has a strong tendency to occupy subsurface or bulk coordination sites. The presence of $Ni^{2+}$ in the mixed aluminates leads to an enhanced surface segregation of $Cu^{2+}$ accompanied by an increased tetrahedral site population by $Cu^{2+}$. The samples are reduced *in vacuo* ($<1.3 \times 10^{-2}$ N $m^{-2}$) at 953 K to form small $Cu_2O$ particles supported on alumina, while $Ni^{2+}$ is not reduced. $H_2$ reduction at 953 K leads to supported metal particles of high dispersion. Copper in the surface layer is nearly quantitatively reduced, while only a small percentage of the total nickel is reduced under these conditions. The reduced nickel does not yield individual pure nickel particles, but forms copper–nickel alloy particles of high dispersion; this leads to an increased adsorption capacity for CO accompanied by the creation of additional chemisorption states. On reoxidation, the original spinel phases can be restored under surprisingly mild conditions. This suggests that the highly disperse metal and oxide phases possess unique properties which strongly deviate from those of bulk phases.

## 1. INTRODUCTION

Cupric ions dispersed on alumina supports are being used as catalysts for a variety of reactions (*1*) and have therefore found extensive interest for fundamental studies regarding the solid state and surface chemistry of the system. The relevant literature has been summarized in a recent contribution (*2*) which mainly concerned a characterization of these catalysts by X-ray photoelectron spectroscopy.

Copper-containing catalysts are active for NO reduction (*3*, *4*). At present, mainly noble metal catalysts are being used for this reaction. However, due to the limited resources of noble metals and because of economic and perhaps political reasons, base metals seem to find renewed interest as NO reduction catalysts. It has recently been shown (*3*) that small amounts of NiO (~1 wt%) increases the activity and stability of dispersed CuO on $Al_2O_3$ and the catalytic behavior of "$Cu–Ni/Al_2O_3$" catalysts as compared to "$Rh/Al_2O_3$" has been studied by Ohara (*4*). We therefore initiated research with the aim of understanding the action of NiO as a promoter. XPS data have already been reported (*2*) and in the present paper, we report on optical spectroscopic and magnetic susceptibility studies and on thermal desorption and infrared spectroscopy of carbon monoxide adsorption on $CuAl_2O_4$ and NiO-promoted $CuAl_2O_4$. These studies include investigations of the reduction and reoxidation behavior of the aluminates.

## 2. EXPERIMENTAL

*2.1. Catalyst preparation.* The $\gamma$-$Al_2O_3$ support was obtained from CATAPAL SB (Südchemie AG, Moosburg, West Germany) by calcination at 1073 K for 15 h. The BET $N_2$ surface area of this support material was 70 $m^2/g$. The catalysts were prepared by impregnation of the support with aqueous solutions of $Cu(NO_3)_2$ or $Ni(NO_3)_2$, or appropriate mixtures of the two nitrates, the concentrations of which

[1] To whom correspondence should be addressed.



0021-9517/81/060475-12$02.00/0

were adjusted so that the final catalysis contained a nominal concentration of 10% wt of CuO or NiO or of 10% wt CuO and additionally 1, 3, or 5% wt NiO. The aqueous suspensions were dried at 400–420 K under vacuum ($< 10^3$ N m$^{-2}$) and subsequently calcined at 1073 K in air for 15 h. The high calcination temperature had to be chosen to ensure aluminate formation. $CuAl_2O_4$ has been shown to be thermodynamically unstable relative to $Al_2O_3$ and CuO at temperatures <870 K at an $O_2$ partial pressure of $2 \times 10^4$ N m$^{-2}$ (*5*). The catalysts obtained show a spinel structure as determined by XRD and XPS (*2*) and by optical diffuse reflectance spectroscopy (see Section 3.11). Possible CuO and/or NiO formation remained below the limits of detectability. The catalysts are designated 10CuAl, 10NiAl, and $x$Ni10CuAl ($x$ = 1,3, and 5) in the following, where the numbers indicate the nominal concentrations in % wt of the transition metal oxides in the aluminate. Exact compositions as determined electrolytically (Cu) and gravimetrically (Ni) and $N_2$ BET surface areas $S_{BET}$ of the catalysts in their oxide state are summarized in Table 1.

The gases used for catalyst treatments or adsorption were from Linde AG: $N_2$ (99.9995%), $O_2$ (99.995%), $H_2$ (99.9995%), and CO (99.997%). They were used without further purification.

*2.2. Diffuse reflectance spectroscopy.* Spectra in the near uv, visible, and near ir region (350–1700 nm) were recorded using the diffuse reflectance technique. The spectrometer used was a Beckman Reflectospectrometer type DK 2A, and the reference white standard was $BaSO_4$. The quartz cells used provided an effective sample thickness of 1 mm, which permits the determination of $R_\infty$ (the reflectance at infinite sample thickness) in the wavelength region studied. The spectra were evaluated by means of the Kubelka–Munk–Schuster function $F(R_\infty)$ (*6*).

TABLE 1

Catalyst Compositions and Surface Areas

| Catalyst | wt% | | $S_{BET}$ (m$^2$/g) |
|---|---|---|---|
| | CuO | NiO | |
| 10CuAl | 10.28 | — | 75 |
| 1Ni10CuAl | 9.84 | 0.97 | 78 |
| 3Ni10CuAl | 10.23 | 2.84 | 76 |
| 5Ni10CuAl | 9.73 | 4.65 | 76 |
| 10NiAl | — | 8.96 | 80 |

*2.3. Magnetic susceptibility measurements.* Magnetic susceptibilities have been measured by means of the Faraday method (*7, 8*). The experimental set-up, which uses a Sartorius vacuum microbalance type 4434, was described in detail elsewhere (*9*). The system was calibrated with $CoHg(SCN)_4$ according to Figgis and Nyholm (*10*). Diamagnetic contributions of the sample holder and the weight loss of samples on evacuation have been taken into account. Measurements were carried out in the magnetic field strength region of 4–7 kG and the temperature range between 300 and 77 K. Contributions of ferromagnetic impurities have been accounted for according to the Honda–Owen (*11*) method. The experimental uncertainty of the gram susceptibility was less than 0.003 cm$^3$/g.

*2.4. Gravimetric adsorption measurements.* Surface areas and CO adsorption have been measured by means of a Sartorius vacuum microbalance type 4102. The system allowed for *in situ* sample treatment.

When necessary, buoyancy corrections have been made. The accuracy of the weight measurements was 2%, and the sample temperature could be controlled within ±2 K.

*2.5. Temperature programmed desorption.* The conventional thermal desorption technique using helium as a carrier gas has been applied. The heating rate was typically 15 K min$^{-1}$. A thermal conductivity cell and a quadrupole mass spectrometer, which were connected via a jet-separator, were used as detectors. Corrections for delay times and for the mass-specific sepa-

ration efficiency of the jet-separator have been made. Details of the experimental set-up and of the data evaluation and correction procedures will be published elsewhere (*12*).

*2.6. ir-transmission spectroscopy.* ir-transmission spectra were measured with a Perkin–Elmer spectrophotometer type 225. The *in situ* cells used have been described previously (*13*). Typically, the spectral slit width in the OH stretching region was 5 $cm^{-1}$, 3 $cm^{-1}$ in the 2500–2000 $cm^{-1}$ range and 1.5 $cm^{-1}$ below 2000 $cm^{-1}$. Self-supporting wafers of the catalysts were obtained by pressing the powder at 250 $kp/cm^2$, their weight being (13 ± 1.5) $mg/cm^2$.

## 3. RESULTS AND DISCUSSION

### *3.1. Characterization of Oxidized Catalysts*

*3.11. Diffuse reflectance spectra.* Figure 1 shows the diffuse reflectance spectra of $\gamma$-$Al_2O_3$, 10CuAl, and 10NiAl. The weak band near 1340 nm of $\gamma$-$Al_2O_3$ has to be assigned to the unresolved first overtone of surface hydroxyl groups. This same band also appears at approximately the same position in all catalysts. Sample 10CuAl shows two principal bands at 1415 and 740 nm, the positions of which compare well with those reported by Freeman and Friedman (*14*) and by Reinen (*15*). These two bands have to be assigned to electronic transitions in $Cu^{2+}$ in tetrahedral

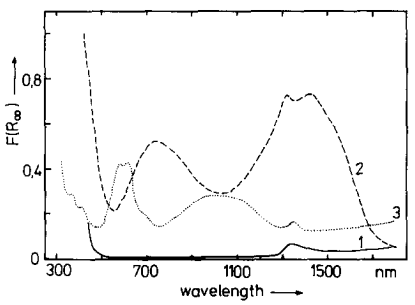


FIG. 1. Diffuse reflectance spectra of (1) $\gamma$-$Al_2O_3$, (2) 10CuAl, and (3) 10NiAl in their oxide forms.

[$^2B_2(^2T_2) \rightarrow {}^2A_1(^2E)$, $^2B_1(^2E)$] and octahedral [$^2B_{1g}(^2E_g) \rightarrow {}^2B_{2g}(^2T_{2g})$, $^2E_g(^2T_{2g})$] sites of the spinel lattice, respectively (*14, 15*). Also 10NiAl shows the characteristic transitions of $Ni^{2+}$ in a spinel matrix (*15*) with the $t_3$ band ($^3T_1 \rightarrow {}^3T_1$) occurring at 586 and 621 nm, the splitting being probably due to spinorbit coupling. However, weak contributions to this band pair from the $O_2$ band ($^3A_{2g} \rightarrow {}^3T_{1g}$) at about 590 nm also exist. The broad band in 10NiAl with center at about 1000 nm corresponds to the $O_1$ band ($^3A_{2g} \rightarrow {}^3T_{2g}$). The reflectance spectra of the two samples 10CuAl and 10NiAl are in agreement with reported spectra of $Cu^{2+}$ and $Ni^{2+}$ in tetrahedral and octahedral interstices of the oxygen lattice. They lend support to previously reported XRD and XPS results, which had suggested the exclusive presence of aluminate phases (*2*).

The tetrahedral band of $Cu^{2+}$ in the mixed systems is found at slightly higher wavelength, namely at 1450 nm. The $t_3$ band of tetrahedral $Ni^{2+}$ is not detected in these catalysts, suggesting that the population of tetrahedral interstices by $Ni^{2+}$ must remain below the limits of detectability when $Cu^{2+}$ is present in the matrix. Simultaneously the extinction ratio at band maximum $E(1450)/E(750)$ of the tetrahedral and octahedral $Cu^{2+}$ bands increases drastically with increasing $Ni^{2+}$ content, as demonstrated in Table 2. This result suggests that the $Cu^{2+}$ ions are forced to occupy tetrahedral sites with increasing preference as the $Ni^{2+}$ content of the samples increases. An explanation of this trend must consider the high octahedral site preference of $Ni^{2+}$ as a $d^8$ ion.

*3.12. Magnetic susceptibility.* The contributions of the various components of the catalysts to the experimental gram susceptibility $\chi_{exp}$ have been calculated from the equation:

$$\chi_{exp} = a\chi_{Cu} + b\chi_{Ni} + c\chi_{Al_2O_3},$$

where the coefficients $a$, $b$, and $c$ are the weight percentages of the individual com-

TABLE 2

Extinction Ratios $E(1450)/E(750)$ of the Tetrahedral and Octahedral $Cu^{2+}$ Bands

| Sample | 10CuAl | 1Ni10CuAl | 3Ni10CuAl | 5Ni10CuAl |
|---|---|---|---|---|
| $E(1450)/E(750)$ | 2.1 | 2.6 | 9.2 | 15.6 |

ponents. The diamagnetic contributions of the oxygen ions corresponding to the transition metal oxide have been neglected, since their value would be lower than $\chi_{exp}$ by three orders of magnitude. Table 3 summarizes the experimental results of the $Cu^{2+}$-containing catalysts, where the Curie constants $C$ and the effective magnetic moments $n_{eff}$ refer to $Cu^{2+}$. The values for 10NiAl are also included for comparison. Ferromagnetic impurities were estimated to be of the order of 10 ppm in all cases.

For sample 10NiAl, the percentage of $Ni^{2+}$ ions in tetrahedral sites could be calculated to be 6.9%, when values of 2.10 and 1.10 were used for Curie constants (*16*) of $Ni^{2+}$ in tetrahedral and octahedral interstices, respectively. Analogous calculations for $Cu^{2+}$ are not possible since the Curie constants for $Cu^{2+}$ in both coordinations are nearly identical because of the Jahn–Teller effect. However, the experimental values of $C$ and $n_{eff}$ compare very well with those reported by Selwood and Dallas (*17*) and Jacobsen and Selwood (*18*), and also with those found for surface spinels by LoJacono (*19*). The latter author reported effective magnetic moments for $Cu^{2+}$ between 1.89 and 1.96 B.M. for samples containing between 0.5 and 10 wt% CuO after calcination at 870 K. The Weiss temperatures varied between −17 and −34 K.

TABLE 3

Magnetic Data of the Aluminates

| Catalyst | Weiss temperature $-\Theta$(K) | Curie constant $C$ | Effective magnetic moment $n_{eff}$ (B.M.) |
|---|---|---|---|
| 10CuAl | $39._7$ | $0.41_3$ | $1.8_4$ |
| 1Ni10CuAl | $61._0$ | $0.38_8$ | $1.7_7$ |
| 3Ni10CuAl | $77._8$ | $0.39_9$ | $1.8_1$ |
| 5Ni10CuAl | $77._2$ | $0.41_2$ | $1.8_3$ |
| 10NiAl | $6._1$ | $1.16_9$ | $3.0_9$ |

The data in Table 3 demonstrate that the Curie constants and effective magnetic moments for $Cu^{2+}$ in the mixed catalysts are practically constant and equal to the values of pure 10CuAl. This is not surprising despite the redistribution of $Cu^{2+}$ ions in the $Ni^{2+}$-containing catalysts, since the Curie constants are identical for $Cu^{2+}$ in tetrahedral and octahedral interstices. The Weiss temperatures on the other hand decrease from −39.7 K for 10CuAl to −77.8 K for 3Ni10CuAl, which suggests the occurrence of an increasing magnetic interaction. This can be explained as follows. First, the total transition metal concentration is increased as $Ni^{2+}$ is added. This, however, cannot account for the overall effect, since $\Theta$ does not decrease further for 5Ni10CuAl. A second and more important reason for the changes of $\Theta$ are different transition metal distributions. Previous XPS studies (*2*) have shown that $Ni^{2+}$ has a strong tendency to penetrate into the bulk. As a result, the $Ni^{2+}$ ions must be highly diluted in the spinel matrix, which leads to vanishing dipolar interactions and to a $\Theta$ value close to zero. The $Cu^{2+}$ ions, on the other hand, showed a tendency to concentrate in the surface layer, which must lead to a much less diluted cation distribution and, hence, a more negative $\Theta$ value. The addition of $Ni^{2+}$ enhances this surface segregation of $Cu^{2+}$ (*2*) (see also Sections 3.13 and 3.14), which as consequence must lead to increased dipolar interactions and more negative Weiss temperatures. The magnetic properties of these catalysts are therefore in good agreement with the structural picture which had been deduced from XPS results (*2*) and for which the infrared studies described in Section 3.14 provide further support.

*3.13. Carbon monoxide adsorption and temperature programmed desorption.* For the gravimetric measurements, the cata-

lysts were treated in $1.3 \times 10^4$ N $m^{-2}$ $O_2$ for 13 h at 953 K and then evacuated at the same temperature to 0.1 N $m^{-2}$ for 1 h. These conditions do not lead to any detectable surface reduction as shown by carbonyl infrared spectra of adsorbed CO (see Section 3.14).

The CO adsorption isotherms at 284 K show a steep increase at low pressures and a saturation region which begins at approximately (6 to 13) $\times$ $10^2$ N $m^{-2}$ for $Cu^{2+}$-containing samples. The saturation capacity of 10CuAl corresponds to $4.2 \times 10^{17}$ molecules/$m^2$, while that of 10NiAl is lower by a factor of approximately five. This result is to be explained by the fact that coordinatively unsaturated $Cu^{2+}$ ions are being exposed in the spinel surface to a much higher extent than $Ni^{2+}$ ions as demonstrated by Shelef *et al.* (*20*) by ion scattering spectroscopy. The same authors had also shown that the NO adsorption capacity of $CuAl_2O_4$ was significantly higher than that of $NiAl_2O_4$.

The addition of $Ni^{2+}$ leads to an increase in CO adsorption capacity; the saturation capacity of sample 1Ni10CuAl at 287 K amounts to $7.2 \times 10^{17}$ molecules/$m^2$. An increased number of exposed transition metal sites must therefore be available in these materials as compared to 10CuAl.

At higher temperatures (<370 K), the adsorption capacities increase in all cases due to carbonate and bicarbonate formation, which is unlikely at 284 K.

Some of the abovementioned trends are also reflected by thermal desorption spectra (TPD) after isothermal CO adsorption at 308 K (*in situ* sample treatment was the same as for the gravimetric measurements). Comparison of the thermal desorption spectra in Fig. 2 confirms the much smaller CO retention on 10NiAl than on the $Cu^{2+}$-containing samples (note the expanded ordinate for sample 10NiAl). Moreover, the CO desorption peak for 10NiAl shows a temperature maximum at 356 K and is relatively narrow, while on $Cu^{2+}$-containing samples the temperature maxima are found between 370 and 403 K and CO desorbs over a wide temperature range up to about 700 K. Activation energies of desorption of CO must therefore be higher and nonuniform on 10CuAl derived samples as compared to 10NiAl. Carbon dioxide is also evolved from $Cu^{2+}$-containing samples, which agrees with the detection of carbonate and bicarbonate species by ir spectroscopy on CO adsorption at temperatures above room temperature (see Section 3.14). Probably, however, the CO will also lead to a surface reduction during thermal desorption, which obviously does not occur on 10NiAl at temperatures below 550 K, in agreement with the difficult reduction of nickel aluminates. These observations agree with the previously reported reduction behavior of the catalysts as studied by XPS (*2*). Additional details of thermal desorption experiments will be discussed elsewhere (*21*).

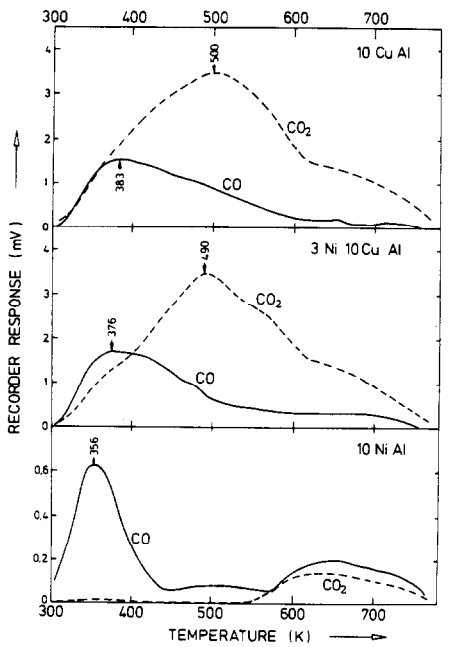


FIG. 2. Thermal desorption spectra (TPD) of CO from oxidized 10NiAl, 10CuAl, and 3Ni10CuAl.

*3.14. Carbon monoxide adsorption: infrared spectroscopy.* After vacuum treatment at 953 K of the $\gamma$-$Al_2O_3$ support, the

five typical OH stretching bands (*22*) could clearly be discerned at 3690, 3725, 3738, 3775, and 3795 $cm^{-1}$. Carbon monoxide adsorption at the sample temperature in the ir beam strongly reduces the intensity of the OH stretching band at 3775 $cm^{-1}$ and leads to the appearance of bands at 3620, 1640, 1484, and 1233 $cm^{-1}$ in agreement with published data (*23–25*). This set of bands is to be assigned to surface bicarbonate species (*23–25*). The origin of an additional band at 1790 $cm^{-1}$ is much disputed in the literature (*23, 26, 27*) and cannot yet be assigned unequivocally. At $1.3 \times 10^3$ N $m^{-2}$ CO pressure, a weak broad band occurs at 2233 $cm^{-1}$ which is due to the carbonyl stretching vibration of CO $\sigma$-coordinated to coordinatively unsaturated $Al^{3+}$ ions (*26, 28*).

The OH stretching bands on the aluminate samples are observed at almost the same wavenumbers as on the alumina support, though their intensities appear to be lower. This suggests that most of the surface hydroxyls retained after vacuum treatment at 953 K should be coordinated to $Al^{3+}$ ions.

Bicarbonate formation is observed on the $Cu^{2+}$-containing aluminates. Bicarbonate species are probably generated by interaction of $CO_2$ with OH groups. The formation of $CO_2$ during CO adsorption suggests at least a slight surface reduction, which would modify the oxidation state of transition metal ions in the surface. In fact, a slight surface reduction by CO would be in agreement with XPS results (*2*). The degree of reduction, however, remains low under the experimental conditions (room temperature) and cannot be detected in the carbonyl stretching region (see below).

In agreement with results reported by Morrow and Moran (*29*), no bicarbonate formation was detected under the applied experimental conditions on the pure sample 10NiAl. The absence of any detectable $CO_2$ evolution at low temperatures during thermal desorption experiments (see Section 3.13 and Fig. 2) and the strong resistance of this sample toward CO reduction at low temperatures (*2*) coincides with these infrared results.

CO is preferentially bound to coordinatively unsaturated $Cu^{2+}$ and/or $Ni^{2+}$ ions in the aluminate surfaces. The respective carbonyl stretching bands develop with increasing CO pressure. For the sake of brevity, only those spectra are reported which were observed at $1.3 \times 10^3$ N $m^{-2}$ CO pressure at the temperature of the sample in the ir beam. The intensities of the carbonyl stretching bands have reached their saturation value under these conditions.

The corresponding carbonyl infrared spectra of samples 10NiAl, 10CuAl, 1Ni10CuAl, 3Ni10CuAl, and 5Ni10CuAl are shown in Fig. 3 (sample pretreatment was the same as described in section 3.13). Wafers of identical weight and size have been used for these experiments so that identical surface areas were exposed to the

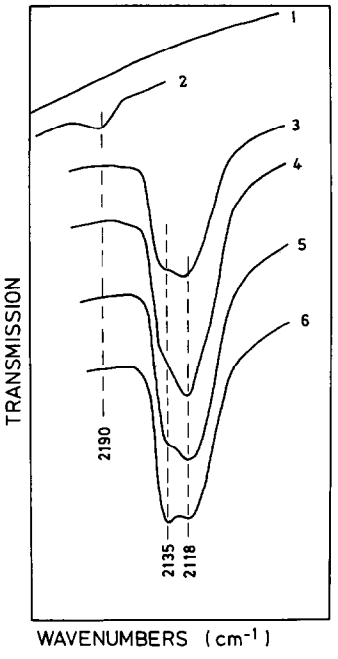


FIG. 3. Infrared carbonyl spectra of oxidized catalysts under $1.3 \times 10^3$ N $m^{-2}$ CO pressure: (1) background; (2) 10NiAl; (3) 10CuAl; (4) 1Ni10CuAl; (5) 3Ni10CuAl; (6) 5Ni10CuAl.

infrared beam and band intensities can be compared on a quantitative basis. 10NiAl only leads to a weak band at 2190 $cm^{-1}$, which is to be assigned to CO coordinated to exposed $Ni^{2+}$ ions (*30*). The low band intensity suggests only a small number of adsorption sites to exist in agreement with the low adsorption capacity of this material (see Section 3.13 and Ref. (*20*)) and with previously reported XPS data (*2*). On the contrary, an intense carbonyl band shows up on sample 10CuAl which is composed of two individual bands centered at 2118 and 2135 $cm^{-1}$. Thus, $Cu^{2+}$ ions must be exposed in the surface of the aluminates at significantly higher density than $Ni^{2+}$ ions, which again agrees with the higher adsorption capacity of 10CuAl and with the surface enrichment of $Cu^{2+}$ as detected by XPS (*2*).

The addition of $Ni^{2+}$ clearly increases the integral band intensity of this doublet band, while no bands in the 2190 $cm^{-1}$ region, which would indicate the exposure of $Ni^{2+}$ in those samples, can be detected. Thus, $Ni^{2+}$ obviously has a tendency to penetrate into the bulk and to lead to an increased surface enrichment of $Cu^{2+}$. These trends had already been observed to occur within the information depth of XPS experiments (30–40 Å) and are supported by the magnetic measurements, while the present infrared adsorption studies confirm that these effects do actually also take place within the surface layer.

The two carbonyl stretching bands observed at 2118 $cm^{-1}$ and 2135 $cm^{-1}$ for CO coordinated on to $Cu^{2+}$ ions are assigned to surface carbonyls with $Cu^{2+}_{tet}$ in tetrahedral and $Cu^{2+}_{oct}$ in octahedral sites, respectively. Borello *et al.* (*30*) had analogously assigned a high-frequency carbonyl band to $Ni^{2+}_{tet}$ in Ni-surface spinels. An unequivocal argument for this assignment on the basis of the carbonyl bond character in the two surface carbonyl species cannot be given at present. However, the extinction ratios calculated from the reflectance spectra and their variation with increasing $Ni^{2+}$ content (see Table 2) lend some support to this assignment.

The carbonyl spectra of sample 1Ni10CuAl (Fig. 3, spectrum 4) show that on addition of small amounts of $Ni^{2+}$ the intensity of the band at 2118 $cm^{-1}$ is preferentially increased. This correlates with the increased tetrahedral site occupation as detected by the reflectance spectra. It is therefore most probably correct to assign the low-frequency carbonyl band to a surface carbonyl with $Cu^{2+}_{tet}$. Infrared carbonyl spectra and $Cu^{2+}$ diffuse reflectance spectra would then consistently describe the $Cu^{2+}$ redistribution in the presence of $Ni^{2+}$ in the spinel lattice. This redistribution with preferential occupation of tetrahedral interstices would be in agreement with the octahedral site preference of $Ni^{2+}$.

### *3.2. Vacuum Reduction*

*In situ* vacuum treatment of the catalysts at 953 K for 13 to 14 h at $1.3 \times 10^{-2}$ N $m^{-2}$ leads to a color change from light green to a dark olive green. XPS studies had indicated a surface reduction at least within the electron escape depth under comparable conditions (*2*); although the Cu oxidation state could not be unequivocally determined from the XPS data, since the $2p_{3/2}$ binding energies of $Cu^0$ and $Cu^{1+}$ are identical, it had been suggested that highly disperse $Cu_2O$ had been formed in the surface layer. Infrared carbonyl spectra support this suggestion. Figure 4 shows the carbonyl stretching bands obtained after adsorption of CO at $1.3 \times 10^3$ N $m^{-2}$ on the vacuum reduced samples. The dominant band in all spectra is observed at 2125 $cm^{-1}$. An additional feature occurs at 2170 $cm^{-1}$. The 2125 $cm^{-1}$ band can be assigned to the stretching vibration of CO coordinated to $Cu^{1+}$ species and it is assumed in agreement with the previous XPS study that $Cu^{1+}$ is present in the form of disperse $Cu_2O$ supported on $Al_2O_3$, since the $Cu^{1+}$ oxidation state can hardly be stabilized in a spinel lattice. Pearce (*31*) had observed the CO stretching vibration near 2130 $cm^{-1}$ on $Cu_2O$. The

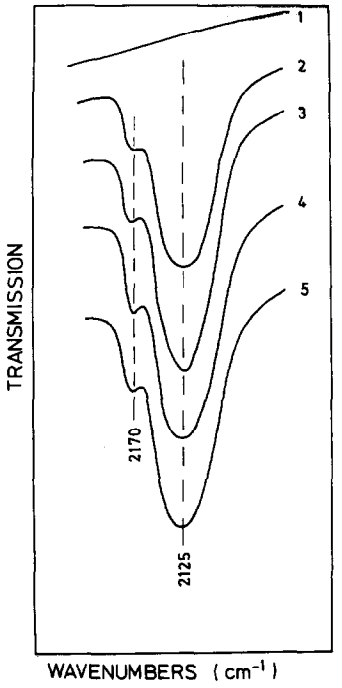


FIG. 4. Infrared carbonyl spectra of vacuum reduced catalysts under $1.3 \times 10^3$ N m$^{-2}$ CO pressure: (1) background; (2) 10CuAl; (3) 1Ni10CuAl; (4) 3Ni10CuAl; (5) 5Ni10CuAl.

weaker band at 2170 cm$^{-1}$ is assigned to Cu–CO$^+$ species (*32, 33*), which can be easily removed on evacuation. Bands indicating the formation of zerovalent Cu (~2100 cm$^{-1}$, see Section 3.3) or Ni (2070 cm$^{-1}$, see Section 3.3) are not detected.

The integral intensity of the 2125 cm$^{-1}$ band increases with increasing Ni content of the samples, which again supports the enhanced surface concentration of Cu in Ni-containing catalysts.

It is interesting to mention here again that the combined use of XPS and infrared spectroscopy (using CO as a probe molecule) allows for an unequivocal distinction between Cu in its Cu$^0$ and Cu$^{1+}$ oxidation states which is not possible on the basis of XPS binding energies alone. On the other hand, the distinction between Cu$^{2+}$ and Cu$^{1+}$ appears to be difficult on the basis of the CO stretching frequencies but it is very easy by means of their respective XPS binding energies (*2*).

Bicarbonate formation is not detected on the vacuum reduced samples. However, weak bands form on CO adsorption at 1550 and 1390 cm$^{-1}$. These bands can be assigned to the antisymmetric and symmetric stretching vibrations of a monodentate surface carbonate species, probably adsorbed on the support alumina. However, there may also be contributions from a surface carboxylate as suggested by London and Bell (*32*).

### *3.3. Reduction in Hydrogen*

*In situ* $H_2$ reduction has been carried out in $1.3 \times 10^4$ N m$^{-2}$ $H_2$ at 953 K. During a period of 13 to 14 h the $H_2$ atmosphere was exchanged several times and the samples were finally evacuated at 953 K for 20 min. XPS had detected exclusively zerovalent Cu$^0$ in 10CuAl after comparable treatments, while only 20% reduction to Ni$^0$ was observed in the 10NiAl sample (*2*).

Carbonate and bicarbonate species are not formed during CO adsorption on the $H_2$ reduced catalysts. Correspondingly, $CO_2$ evolution is not observed from these samples during thermal desorption experiments after CO adsorption at 308 K (Fig. 5). The adsorption capacity for CO is strongly reduced as compared to the oxidized samples, in particular 10CuAl, although the $N_2$ BET surface areas are identical for the

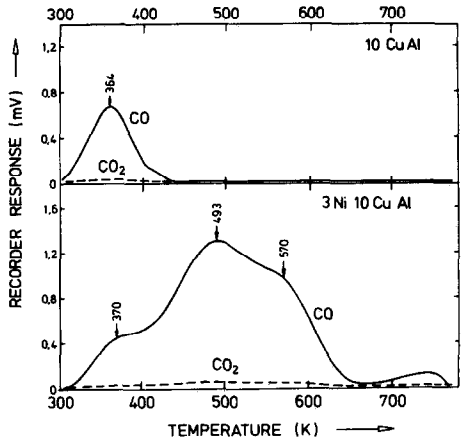


FIG. 5. Thermal desorption spectra (TPD) of CO from $H_2$-reduced catalysts 10CuAl and 3Ni10CuAl.

reduced and oxidized samples. A symmetrical desorption peak with maximum at 364 K is observed. The desorption trace differs significantly from this one in the presence of nickel as shown in Fig. 5 for sample 3Ni10CuAl. The typical desorption peak at 364 K observed for 10CuAl seems to be reduced in peak height while two additional desorption peaks appear with maxima at 493 and approximately 570 K, indicating two more strongly bound CO chemisorption states in the Ni-containing sample. Thus, on comparison with Fig. 2 it turns out that the CO chemisorption capacity is lower on the reduced than on the oxidized samples. Most significantly, the presence of Ni in the reduced samples enhances the CO adsorption with respect to adsorption capacity and activation energy for desorption. Thus, the relatively small proportion of Ni being reduced in the systems seems to yield a better dispersion of the metal phase with a larger number of energetically different adsorption sites being exposed.

Thermal desorption from the $H_2$ reduced sample 10NiAl could not be carried out, since an extremely hazardous $Ni(CO)_4$ formation occurred during isothermal CO adsorption at room temperature. Most interestingly this was not observed on the reduced Cu-containing samples. Obviously the presence of Cu reduced the $Ni(CO)_4$ formation below the limits of detectability.

Carbonyl infrared spectra of the $H_2$-reduced samples 10CuAl, 1Ni10CuAl, 3Ni10CuAl, and 5Ni10CuAl after adsorption of $1.3 \times 10^4$ N $m^{-2}$ CO at the sample temperature in the infrared beam are reported in Fig. 6. In all cases the bands of CO coordinated to $Cu^{2+}_{oct}$ and $Cu^{2+}_{tet}$ are observed, although at strongly reduced integral band intensity as compared to the oxidized samples. Thus, the samples are not reduced completely and a few $Cu^{2+}$ coordination sites have remained on the surface. The relative band intensities of CO on $Cu^{2+}_{oct}$ and $Cu^{2+}_{tet}$ as compared to the oxidized samples (Fig. 3) suggest that the $Cu^{2+}$ ions in tetrahedral sites are much more easily reduced than those in octahedral sites.

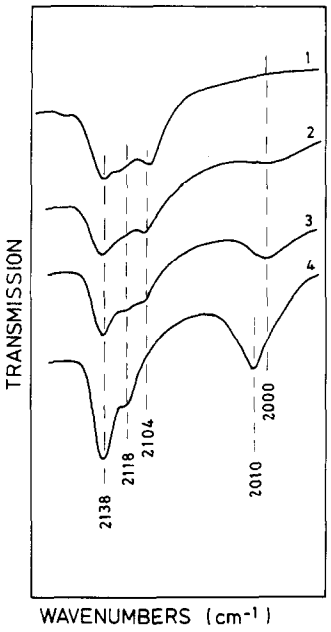


FIG. 6. Infrared carbonyl spectra of $H_2$-reduced catalysts under $1.3 \times 10^3$ N $m^{-2}$ CO pressure: (1) 10CuAl; (2) 1Ni10CuAl; (3) 3Ni10CuAl; (4) 5Ni10CuAl.

On 10CuAl an additional band is observed at 2097 $cm^{-1}$, which is clearly assigned to CO adsorbed on zerovalent metallic copper (*34–36*). The Ni-containing samples do not show any carbonyl bands of CO adsorbed on metallic nickel which would be expected between 2040 and 2070 $cm^{-1}$ (*36*). Only the pure 10NiAl sample (not shown in Fig. 6) shows a weak band in this region after $H_2$ reduction. However, the mixed catalysts in their reduced form develop a broad band between 2000 and 2010 $cm^{-1}$, the intensity of which increases with increasing Ni-content of the oxidized percursor sample and the position of which shifts from 2000 $cm^{-1}$ in 1Ni10CuAl to 2010 $cm^{-1}$ in 5Ni10CuAl. Simultaneously the typical band of CO adsorbed on pure metallic copper shifts slightly to higher wavenumbers and is reduced in intensity. This band has completely vanished on sample 5Ni10CuAl.

These observations suggest the formation of small Cu–Ni alloy particles besides pure Cu particles on samples 1Ni10CuAl and 3Ni10CuAl, while on sample 5Ni10CuAl pure Cu particles do not seem to exist. Ni-metal particles are not being formed at all. These assignments agree with those put forward in the literature (*37, 38*), namely by Soma-Noto and Sachtler (*37*) and by Dalmon *et al.* (*38*). The latter two groups reported carbonyl infrared bands near 2000 $cm^{-1}$ for CO adsorption on copper-rich Cu–Ni alloys containing only a few percent Ni. The band shifts to higher wavenumbers as the Ni content in the alloy is increased (*38*).

The present results suggest that the reduction of the mixed aluminate phases leads to small metallic particles, where the Ni atoms are quantitatively incorporated within Cu–Ni alloy particles; these contain only below 20% Ni as concluded from the carbonyl band position (*38*), this being due to the low degree of reduction of nickel in the catalyst samples (*2*). This alloying obviously has a remarkable effect on the CO retention and heat of adsorption of CO as shown by the thermal desorption spectra (Fig. 5). The appearance of additional adsorption states at higher energy in the mixed systems compares qualitatively with thermal desorption spectra of CO from Cu–Ni alloy single crystals, although the activation energies for desorption are significantly lower for the latter systems (*40, 41*).

### *3.4. Reoxidation*

Figure 7 shows the spectral changes in the carbonyl stretching region after CO adsorption at $1.3 \times 10^3$ N $m^{-2}$, when the $H_2$-reduced catalysts, namely 3Ni10CuAl as a typical example, were subjected to $O_2$ treatments at 953 K at various $O_2$ pressures. For direct comparison these spectra have to be compared with spectrum 3 in Fig. 6, which corresponds to the $H_2$-reduced form of the catalyst. After exposure of this reduced catalyst to an $O_2$ atmosphere of $1.3 \times 10^{-2}$ N $m^{-2}$, the intensity of the band at 2000 $cm^{-1}$ is clearly reduced and the carbonyl band of CO on $Cu^0$ is shifted slightly to higher wavenumbers. These trends become more pronounced with time, and after treatment in $1.3 \times 10^{-1}$ N $m^{-2}$ $O_2$ for 12 h spectrum 3 in Fig. 7 is obtained. This spectrum is nearly identical with that obtained for CO adsorbed on supported $Cu_2O$ (see Fig. 4 and Section 3.2) and suggests the reoxidation of the small metal particles. A continued $O_2$ treatment at $1.3 \times 10^4$ N $m^{-2}$ and 953 K leads to a color change from black to the original light olive-green of the oxidized samples. The infrared carbonyl spectra (spectrum 4, Fig. 7) are equivalent to those of the original aluminates (Fig. 3), showing the two characteristic bands at 2135 and 2118 $cm^{-1}$ for CO coordinated to $Cu^{2+}$ in octahedral and tetrahedral sites in the spinel lattice.

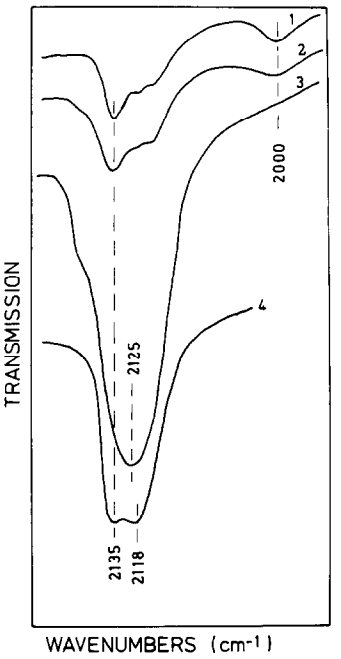


FIG. 7. Infrared carbonyl spectra of 3Ni10CuAl under $1.3 \times 10^3$ N $m^{-2}$ CO pressure at different degrees of reoxidation at 953 K: (1) after 0.3 h in $1.3 \times 10^{-2}$ N $m^{-2}$ $O_2$ pressure; (2) after 2 h in $1.3 \times 10^{-2}$ N $m^{-2}$ $O_2$ pressure; (3) after 12 h in $1.3 \times 10^{-1}$ N $m^{-2}$ $O_2$ pressure; (4) after 13 h in $1.3 \times 10^4$ N $m^{-2}$ $O_2$ pressure.

This suggests a complete reoxidation and

reformation of the original aluminate during this reduction/reoxidation cycle. Most interestingly the aluminate formation occurs under very mild conditions as compared to the original preparation conditions. These observations are in complete agreement with previously reported XPS results (*2*), which had demonstrated that the reoxidation of $H_2$-reduced samples led to the formation in a first step of supported $Cu_2O$, which was then oxidized to yield supported CuO in $1.6 \times 10^4$ N $m^{-2}$ $O_2$ at 470 K. At only 720 K, the supported CuO was transformed quantitatively into the aluminate. It must therefore be concluded that the apparently highly disperse CuO particles and perhaps also the superficial $Al_2O_3$ region which are being formed during reduction–reoxidation cycles exhibit thermodynamic properties that deviate from those of the bulk phases.

The relative intensities of the carbonyl bands of CO coordinated to octahedral and tetrahedral $Cu^{2+}$ after reoxidation (spectrum 4 in Fig. 7) differ from those observed for the original oxidized samples. The $Cu^{2+}$ distribution in the surface must therefore be different in the two samples. It is known that the cation distributions in aluminates depend on the calcination temperature and time and on the humidity of the atmosphere (*30*). For $CuAl_2O_4$ it has particularly been shown (*39*) that the tetrahedral site population increases with calcination time at temperatures above 870 K. Thus, the different sample treatment conditions during catalyst preparation and reoxidation must account for the different $Cu^{2+}$ distributions.

## 4. CONCLUSIONS

Regarding the effect of nickel on the nature and properties of the catalysts, the following conclusions can be drawn from the present results.

(a) In the oxide aluminate samples $Ni^{2+}$ ions have a strong tendency to occupy octahedral sites in subsurface layers and in the bulk. They are hardly exposed in the surface.

(b) The presence of $Ni^{2+}$ leads to a $Cu^{2+}$ redistribution with an increased tetrahedral site population by $Cu^{2+}$.

(c) This $Cu^{2+}$ redistribution is accompanied by an enhanced surface segregation, which leads to an increased number of exposed $Cu^{2+}$ ions in the surface of the aluminates.

(d) On $H_2$ reduction, highly disperse metal particles of unique thermodynamic properties are produced.

(e) $Ni^{2+}$ is only reduced to a small degree (<20%). The reduced Ni atoms are incorporated in small Cu–Ni alloy particles.

(f) The alloy formation also seems to increase the dispersion of the metal phase and induces additional high energy adsorption states for CO.

(g) The alloy formation also prevents the generation of $Ni(CO)_4$ on exposure to CO at low temperature, an observation which may be important with respect to practical application of these catalysts.

It is presumed that these effects should strongly influence the catalytic properties of these materials, namely with respect to the chemisorption and reduction of nitric oxide on which we will report in the near future.

## ACKNOWLEDGMENTS

The financial support of this work by the Deutsche Forschungsgemeinschaft, the Fonds der Chemischen Industrie, the Max-Buchner-Forschungsstiftung, and the Stiftung Volkswagenwerk is gratefully acknowledged. We also wish to thank Mr. J. Abart for his help with the magnetic susceptibility measurements.

## REFERENCES

1. Thomas, C. L., "Catalytic Processes and Proven Catalysts." Academic Press, New York, 1970.
2. Ertl, G., Hierl, R., Knözinger, H., Thiele, N., and Urbach, H. P., *Appl. Surface Sci.* **5**, 49 (1980).
3. Blanco, J., private communication.
4. Ohara, T., *in* "The Catalytic Chemistry of Nitrogen Oxides" (R. L. Klimisch and J. G. Larson, Eds.), p. 191. Plenum Press, New York, London, 1975.
5. Jakob, K. T., and Alcock, C. B., *J. Amer. Ceram. Soc.* **58**, 192 (1975).
6. Kortüm, G., "Reflexionsspektroskopie."

Springer-Verlag, Berlin, Heidelberg, New York, 1969.
7. Weiss, A., "Magnetochemie." Verlag Chemie, Heidelberg, 1973.
8. Selwood, W., "Magnetochemistry." Interscience Publ., London, New York, 1956.
9. Abart, J., Diplomarbeit, University of Munich, 1976.
10. Figgis, B. N., and Nyholm, R. S., *J. Chem. Soc.* 4190 (1958).
11. Bates, L., "Modern Magnetism." Cambridge Univ. Press, 1961.
12. Hierl, R., Knözinger, H., and Schubart, W., to be published.
13. Knözinger, H., Stolz, H., Bühl, H., Clement, G., and Meye, W., *Chem.-Ing.Techn.* **42**, 548 (1970).
14. Freeman, J. J., and Friedman, R. M., *JCS Faraday I* **74**, 758 (1978).
15. Reinen, D., *Struct. Bonding* **7**, 114 (1970).
16. LoJacono, M., Schiavello, M., and Cimino, A., *J. Phys. Chem.* **75**, 1044 (1971).
17. Selwood, P. W., and Dallas, N. S., *J. Amer. Chem. Soc.* **70**, 2145 (1948).
18. Jacobson, P. E., and Selwood, P. W., *J. Amer. Chem. Soc.* **76**, 2641 (1954).
19. LoJacono, M., personal communication.
20. Shelef, M., Wheeler, M. A. Z., and Yao, H. C., *Surface Sci.* **47**, 697 (1975).
21. Hiere, R., and Knözinger, H., to be published.
22. Knözinger, H., and Ratnasamy, P., *Catal. Rev.-Sci. Eng.* **17**, 31 (1978).
23. Parkyns, N. D., *J. Chem. Soc.* (A), 1910 (1967).
24. Little, L. H., and Amberg, C. H., *Canad. J. Chem.* **40**, 1997 (1962).
25. Morikawa, Y., and Amenomiya, Y., *J. Catal.* **54**, 281 (1978).
26. Morterra, C., Zecchina, A., Coluccia, S., and Chiorino, A., *JCS Faraday I* **73**, 1544 (1977).
27. Fink, P., *Z. Chem.* **7**, 324 (1967).
28. Della Gatta, G., Fubini, B., Ghiotti, G., and Morterra, C., *J. Catal.* **43**, 90 (1976).
29. Morrow, B. A., and Moran, L. E., *J. Phys. Chem.* **81**, 2667 (1977).
30. Borello, E., Cimino, A., Ghiotti, G., LoJacono, M., Schiavello, M., and Zecchina, A., *Disc. Faraday Soc.* **52**, 149 (1971).
31. Pearce, H. A., Ph.D. Thesis, University of East Anglia, Norwich, England, 1974.
32. London, J. W., and Bell, A. T., *J. Catal.* **31**, 96 (1973).
33. Gardner, R. A., and Petrucci, R. H., *J. Amer. Chem. Soc.* **82**, 5051 (1960).
34. Tompkins, H. G., and Greenler, R. G., *Surface Sci.* **28**, 194 (1971).
35. Pritchard, J., Catterick, T., and Gupta, R. K., *Surface Sci.* **53**, 1 (1975).
36. Sheppard, N., and Nguyen, T. T., *Adv. Infrared Raman Spectrosc.* **5**, 67 (1978).
37. Soma-Noto, Y., and Sachtler, W. M. H., *J. Catal.* **34**, 162 (1974).
38. Dalmon, J. A., Primet, M., Martin, G. A., and Imelik, B., *Surface Sci.* **50**, 95 (1975).
39. Friedman, R. B., Freeman, J. J., and Lytle, F. W., *J. Catal.* **55**, 10 (1978).
40. Yu, K. Y., Ling, D. T., and Spicer, W. E., *J. Catal.* **44**, 384 (1976).
41. Wandelt, K., personal communication.